LANGMUIR Article
Cite This: Langmuir 2019, 35, 7129−7135
pubs.acs.org/Langmuir

Analytical Expressions for Spring Constants of Capillary Bridges and Snap-in Forces of Hydrophobic Surfaces

Veikko Sariola*

Faculty of Medicine and Health Technology, Tampere University, Korkeakoulunkatu 3, 33720 Tampere, Finland

Supporting Information

ABSTRACT: When a force probe with a small liquid drop adhered to its tip makes contact with a substrate of interest, the normal force right after contact is called the snap-in force. This snap-in force is related to the advancing contact angle or the contact radius at the substrate. Measuring snap-in forces has been proposed as an alternative to measure the advancing contact angles of surfaces. The snap-in occurs when the distance between the probe surface and the substrate is h_S, which is amenable to geometry, assuming the drop was a spherical cap before snap-in. Equilibrium is reached at a distance $h_E < h_S$. At equilibrium, the normal force $F = 0$, and the capillary bridge is a spherical segment, amenable again to geometry. For a small normal displacement $\Delta h = h - h_E$, the normal force can be approximated with $F \approx -k_1\Delta h$ or $F \approx -k_1\Delta h - k_2\Delta h^2$, where $k_1 = -\partial F/\partial h$ and $k_2 = -1/2\cdot\partial^2 F/\partial h^2$ are the effective linear and quadratic spring constants of the bridge, respectively. Analytical expressions for $k_{1,2}$ are found using Kenmotsu's parameterization. Fixed contact angle and fixed contact radius conditions give different forms of $k_{1,2}$. The expressions for k_1 found here are simpler, yet equivalent to the earlier derivation by Kusumaatmaja and Lipowsky (2010). Approximate snap-in forces are obtained by setting $\Delta h = h_S - h_E$. These approximate analytical snap-in forces agree with the experimental data from Liimatainen et al. (2017) and a numerical method based on solving the shape of the interface. In particular, the approximations are most accurate for super liquid-repellent surfaces. For such surfaces, readers may find this new analytical method more convenient than solving the shape of the interface numerically.

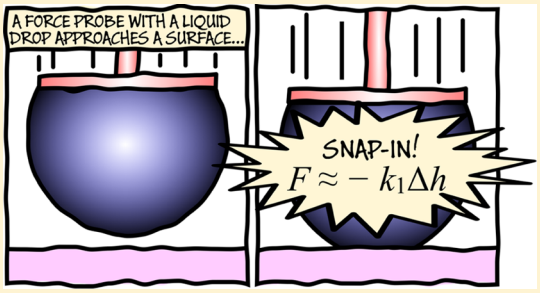

INTRODUCTION

An axisymmetric capillary bridge between two parallel surfaces exerts a normal force on the surfaces. Such capillary bridges are encountered in self-aligning liquid joints,[1−6] capillary grippers,[7−9] capillarity-based switchable adhesive surfaces,[10] granular media,[11] the adhesion of nanoparticles,[12] and soft materials,[13] the adhesion and friction of powders, and biofibers,[14] when using capillary bridges as flexible joints,[15] atomic force microscopy,[16,17] among other applications. These capillary bridges are of particular interest when the normal force is measured to quantify the (super) liquid repellency of the surfaces.[18−20] In a typical force characterization experiment, a force probe with a drop at its tip approaches the substrate of interest, then makes contact with the substrate and finally retracts from the substrate. The force right after the first contact is called the snap-in force, and smaller snap-in forces have been experimentally[20−22] and theoretically[18,20] shown to correspond to larger advancing contact angles and smaller contact radii. Unlike contact angle measurements, the force measurements can remain accurate even when the substrate is super liquid-repellent (e.g., $\theta > 150°$) or when the surface is not flat.[19,20,23]

To theoretically relate a force to the contact angle or contact radius, one has to find the shape of the surface, typically numerically. In a direct version of the problem, one computes the shape of the interface for a known geometry (e.g., liquid bridge height, volume, and contact radius at the probe and contact angle at the substrate) and then computes the force, for example, as a sum of capillary and Laplace pressure terms.[18] In the force characterization experiments, we are actually interested in solving an inverse version of the problem: find the geometry (e.g., contact angle at the substrate, assuming everything else is known) that corresponds to the measured force.

There are several methods for finding the shape of the capillary bridge. One numerical method is to solve the Young−Laplace equation with boundary conditions and a volume constraint.[20] An alternative numerical method is to minimize the energy functional using a finite element method[24] or by optimizing a discrete mesh shape,[25,26] one particularly popular option for the latter being the Surface Evolver[25] software. Finally, when gravity is neglected, all solutions of the Young−Laplace equation are constant-mean-curvature surfaces and the axisymmetric solutions are the Delaunay surfaces:[27] planes, cylinders, spheres, catenoids, nodoids, or unduloids. One parameterization of the Delaunay surfaces was found by Kenmotsu.[28] In principle, the shape of the surface can be found by finding the Kenmotsu parameters for which the constraints

Received: January 15, 2019
Revised: April 9, 2019
Published: April 16, 2019

(volume, contact angles, or contact radii) are fulfilled. Unfortunately, the Kenmotsu parameterization involves elliptic integrals, so the parameters will have to be sought numerically. An analytical method for computing the force, without solving the exact shape of the capillary bridge, would still be highly useful.

An important special case of the Delaunay surfaces is the spherical-segment-shaped capillary bridge. Such bridges can be handled by simple geometry and their Kenmotsu parameters are trivial. This case is especially important because a spherical segment is the equilibrium shape (normal force $F = 0$) of a liquid bridge when gravity is negligible. Furthermore, in many practical applications, the capillary bridges are nearly spherical. We will see that this is the case when computing the snap-in forces of a super liquid-repellent surface (contact angles near 180°) or a pad with a small radius. We use the term pad as a generic term for a circularly patterned substrate on which the liquid completely wets a circular area, but then is pinned to the edge of the area. This can be achieved through surface chemistry (a highly wettable area on a highly liquid-repellent background) or surface topography, for example, a protruding pillar on whose edge the drop pins.

In this paper, the force−distance relationship of an axisymmetric capillary bridge is analytically linearized at the equilibrium distance using the Kenmotsu parameterization and this linearized model is used to estimate the snap-in force. The distance at which the bridge is in equilibrium is denoted with h_E (Figure 1). For a small normal displacement $\Delta h = h - h_E$, the normal force F can be approximated with a first-order approximation

$$F_{\text{linear}} \approx -k_1 \Delta h \tag{1}$$

or a second-order approximation

$$F_{\text{quadratic}} \approx -k_1 \Delta h - k_2 \Delta h^2 \tag{2}$$

where $k_1 = -\partial F/\partial h$ and $k_2 = -1/2 \cdot \partial^2 F/\partial h^2$ are respectively the effective linear and quadratic spring constants of the capillary bridge.

Fixed contact angle and fixed contact radius conditions give different forms of $k_{1,2}$. Kusumaatmaja & Lipowsky[29] identified three different cases (eqs 46−48 in their paper), and we will stick to their labeling:

Case I: both substrates are homogeneous and the contact angles are fixed. The contact angles of the two substrates are not necessarily the same.

Case II: the bottom substrate is homogeneous and its contact angle is fixed, while the top substrate is patterned with a pad and its contact radius is fixed. The roles of the two substrates can be of course chosen freely; we assume that it is the bottom substrate that is homogeneous.

Case III: both substrates are patterned with pads of certain radius, and the liquid fully wets the pads, and contact lines are pinned to the pad edges. In other words, the contact radii on both substrates are fixed although not necessarily the same.

For force characterization experiments, fabricating a force probe surface with a known pad radius is easier than fabricating a force probe surface with a truly homogenous surface with a stable contact angle, so the cases II and III are expected to be more relevant here. The force−distance curves in cases II and III are illustrated in Figure 1a,b, respectively. Nevertheless, for completeness, we will give the spring constants for the three cases.

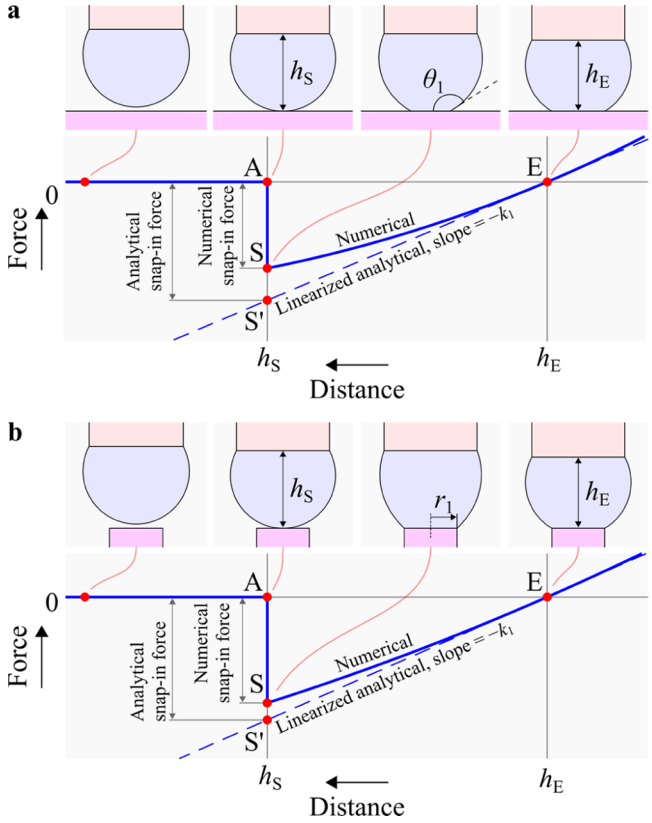

Figure 1. Method for calculating snap-in force analytically for (a) homogeneous substrates, with a constant contact angle; and (b) pads or pillars, with a constant contact radius. Point A is when the tip of the spherical cap-shaped drop touches the substrate. The corresponding distance h_S can be solved using the geometry. Point E is when the capillary bridge is in equilibrium, its shape is a spherical segment and the force is again 0. The corresponding distance h_E can be solved using geometry. Accurate snap-in force (point S) can only be solved numerically, but we can analytically linearize the force curve at point E and use the linearized curve to find point S′, which approximates the snap-in force.

The snap-in occurs at a distance h_S, which is amenable to geometry, assuming the drop was a spherical cap before snap-in. Approximate snap-in forces are finally obtained by setting $\Delta h = h_S - h_E$ (Figure 1). These approximate analytical snap-in forces agree with the experimental data from Liimatainen et al.[20] and a numerical method based on solving the shape of the interface.

Previous Work. Kusumaatmaja & Lipowsky[29] have earlier derived the linear spring constant k_1 in all three cases by starting from the energy functional and then considering small perturbations to the equilibrium shape. The expressions for the spring constants found here are simpler yet equivalent to their derivation.

Meurisse & Querry[30] and Petkov & Radoev[31] computed approximate forces in the case I, with the further assumption that both surfaces have the same contact angle. Meurisse and Querry started from accurate descriptions of Delaunay's surfaces, and then approximated the profile curve with a circular arc. Petkov and Radoev used a numerical procedure, based on parameterization of the profile curves. Furthermore, Vogel[32] studied capillary bridges in the general case I and in particular, derived a general condition for the second-order stability of the capillary bridge.

DOI: 10.1021/acs.langmuir.9b00152
Langmuir 2019, 35, 7129−7135

Escobar & Castillo[19] found the normal force in the case II by minimizing an energy functional.

Heinrich et al.[33] and Goldman[2] computed the forces in the case III. Heinrich simplified the problem by assuming that the profile curve is a circular arc, while Goldman first used numerical methods and then fitted a heuristic equation to the numerical force−distance data.

Attard & Miklavcic[16] computed the spring constants of liquid bubbles when interacting with spherical particles or probes, which is different in geometry from all the three cases considered here. Nevertheless, their spring constant expression has very similar form to the ones derived here, including logarithmic and rational parts, and they underlined that all systems must behave as simple springs for sufficiently small approximations,[16] which is the rationale for the linearization approximation taken here.

More general geometries (square-shaped pads, nonaligned pads, etc.) have been handled numerically by several authors.[1,6,34]

METHODS

In this paper, we make the following assumptions, which are not difficult to fulfill in experimental conditions.

(1) The gravity can be neglected. In practice, this means that the capillary bridges must be small compared to the capillary length, ≈2.7 mm for water in an ordinary room environment.
(2) The capillary bridges are axially symmetric. In practice, this means that both surfaces will have to be parallel in all the three cases. Furthermore, in the case III, the two pads should be axially aligned to each other, but cases I and II are self-aligning in the sense that they can assume an axially symmetric configuration because of energy minimization.
(3) The relative motion of the probe is slow, in the sense that we can ignore the hydrodynamics of the liquid. In other words, for every distance, we can assume that the interface is in equilibrium.
(4) The evaporation of the drop is slow compared to the duration of the experiment, so that we can assume that the volume of the drop is constant.

On both substrates, we assume that either that the contact radius is fixed or the contact angle is fixed (cases I−III), but importantly, we do not assume that the conditions on both substrates are necessarily the same. Figure 2 shows the geometry and symbols used in this paper.

Supporting Information contains a Maple worksheet that shows all the steps taken in the derivation of the theory.

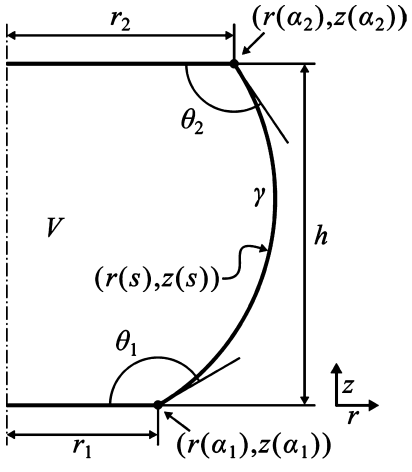

Figure 2. Schematic of the geometry and symbols used in the paper.

Axisymmetric Constant Mean Curvature Surfaces. Recall that the shape of the capillary interface is governed by the Young−Laplace equation

$$2H = \Delta p/\gamma \tag{3}$$

where H is the mean curvature, Δp is the Laplace pressure, and γ is the surface tension of liquid. Neglecting gravity, Δp is constant and the surface has a constant mean curvature of $\Delta p/2\gamma$.

Axisymmetric constant-mean-curvature surfaces are the Delaunay surfaces: planes, cylinders, spheres, catenoids, nodoids, or unduloids.[27] Kenmotsu[28] parameterized the profile curve (r,z) of Delaunay surfaces as

$$r(s) = \frac{1}{2H}\sqrt{1 + B^2 + 2B\sin 2Hs} \tag{4}$$

$$z(s) = \int_0^s \frac{1 + B\sin 2Ht}{\sqrt{1 + B^2 + 2B\sin 2Ht}}\,\mathrm{d}t \tag{5}$$

where B and H control the shape of the interface, H being the mean curvature of the surface, and s is the curve parameter. The surface is an unduloid when $B < 1$ and the surface is an nodoid when $B > 1$. When $B = 1$, the surface is a sphere, and in this case, the radius of the sphere is $R = 1/H$.

For later treatment, we will rewrite 4 and 5 by

(1) Changing sin → cos. This is a matter of preference. It is preferable to have the center of spherical joints at origin, which will simplify the relation between contact angles and the integration limits in 5.
(2) Setting $R = 1/H$. We will not consider the case $H = 0$.
(3) Changing variables $s \to Rs$ and $t \to Rt$
(4) Using the relation $\cos 2x = 2\cos^2 x - 1$

After these manipulations, we get

$$r(s) = \frac{R}{2}\sqrt{(1 - B)^2 + 4B\cos^2 s} \tag{6}$$

$$z(s) = R\int_0^s \frac{(1 - B) + 2B\cos^2 t}{\sqrt{(1 - B)^2 + 4B\cos^2 t}}\,\mathrm{d}t \tag{7}$$

The liquid bridge is an arc of the profile curve with $s \in [\alpha_1,\alpha_2]$, so there are a total of four shape parameters that fully describe the capillary bridge: B, R, α_1, and α_2. Note that R is a simple scaling parameter with a dimension of length, while the rest are nondimensional quantities.

Solving the Shape and Force of the Liquid Bridge. In the case III (both contact radii fixed), we can find the shape parameters by treating volume V, joint height h, and pad radii r_1 and r_2 as the independent variables and B, R, α_1, and α_2 as the dependent variables. The dependent variables can be found by solving a system of equations

$$\begin{aligned} h &= z(\alpha_2) - z(\alpha_1) \\ V &= \pi\int_{\alpha_1}^{\alpha_2} r(t)^2 z'(t)\,\mathrm{d}t \\ r_1 &= r(\alpha_1) \\ r_2 &= r(\alpha_2) \end{aligned} \tag{8}$$

Cases I and II can be found replacing $r_1 = r(\alpha_1)$ with $-\cot\theta_1 = r'(\alpha_1)/z'(\alpha_1)$ or by replacing $r_2 = r(\alpha_2)$ with $\cot\theta_2 = r'(\alpha_2)/z'(\alpha_2)$. Once the dependent variables, that is, the shape of the surface, are known, the normal force F can be found as the sum of Laplace and capillary terms[18]

$$F = \pi {r_1}^2\Delta p - 2\pi\gamma r_1\sin\theta_1 \tag{9}$$

Using $\Delta p = 2\gamma/R$ and the relation $\sin\theta = 1/(1 + r'^2/z'^2)$ with 6 and 7, we get

DOI: 10.1021/acs.langmuir.9b00152
Langmuir 2019, 35, 7129−7135

$$F = \frac{\pi\gamma R(B^2 - 1)}{2} \tag{10}$$

This shows that F depends on B and R, but does not explicitly depend on α_1 or α_2.

Special Case of Spherical Segments. It was already pointed out that the capillary bridge is a spherical segment when $B = 1$. Putting $B = 1$ into (6 and 7), we see that

$$(r, z) = (R\cos s, R\sin s) \tag{11}$$

when $-\pi/2 < s < \pi/2$. Furthermore, from 10 it is clear that when $B = 1$, the force $F = 0$, so the equilibrium shape of a liquid bridge is a spherical segment. Finally, for the case of a spherical segment, α_1 and α_2 are related to the contact angles by

$$\alpha_1 = \pi/2 - \theta_1 \tag{12}$$

$$\alpha_2 = \theta_2 - \pi/2 \tag{13}$$

Using simple geometry,[29] the parameters R, α_1, and α_2 can now be solved depending on the case. This also gives the equilibrium distance h_E.

Linear Spring Constants. Our next goal is to derive the linear spring constant $k_1 = -\partial F/\partial h$ for the equilibrium case $B = 1$. We start by noting that k_1 must be independent of R. This follows from the fact that the dependent variables uniquely define the surface so that $k_1 = k_1(\gamma,B,R,\alpha_1,\alpha_2)$. The units of k_1 and γ are N/m, the unit of R is m and B, α_1, and α_2 are nondimensional quantities so a dimensional argument[35] can be put forward that $k_1/\gamma = \tilde{k}_1(B, \alpha_1, \alpha_2)$ Thus, without loss of generality, we can compute the spring constant in the case $R = 1$.

In the case III, the spring constant is given by (remembering that F does not explicitly depend on α_1 and α_2)

$$k_1 = -\left(\frac{\partial F}{\partial h}\right)_{V,r_1,r_2} = -\left(\frac{\partial F}{\partial B}\right)\left(\frac{\partial B}{\partial h}\right)_{V,r_1,r_2} - \left(\frac{\partial F}{\partial R}\right)\left(\frac{\partial R}{\partial h}\right)_{V,r_1,r_2} \tag{14}$$

When $B = 1$, from 10 we see that $\partial F/\partial R = 0$ so that in this specific case, the second term in 14 can be neglected. To find $\partial B/\partial h$, the implicit function theorem and Cramer's rule can be used to get

$$\left(\frac{\partial B}{\partial h}\right)_{V,r_1,r_2} = \frac{\frac{\partial(V,r_1,r_2)}{\partial(R,\alpha_1,\alpha_2)}}{\frac{\partial(h,V,r_1,r_2)}{\partial(B,R,\alpha_1,\alpha_2)}} \tag{15}$$

where $\partial(...)/\partial(...)$ denotes the Jacobian determinant. For the numerator, evaluating at $B = 1$ and $R = 1$ gives

$$\begin{aligned}
&\left.\frac{\partial(V,r_1,r_2)}{\partial(R,\alpha_1,\alpha_2)}\right|_{B=1,R=1} \\
&= \left.\begin{vmatrix} \partial V/\partial R & \partial V/\partial\alpha_1 & \partial V/\partial\alpha_2 \\ \partial r_1/\partial R & \partial r_1/\partial\alpha_1 & \partial r_1/\partial\alpha_2 \\ \partial r_2/\partial R & \partial r_2/\partial\alpha_1 & \partial r_2/\partial\alpha_2 \end{vmatrix}\right|_{B=1,R=1} \\
&= \begin{vmatrix} 3\pi\int_{\alpha_1}^{\alpha_2}\cos^3 t\,dt & -\pi\cos^3\alpha_1 & \pi\cos^3\alpha_2 \\ \cos\alpha_1 & -\sin\alpha_1 & 0 \\ \cos\alpha_2 & 0 & -\sin\alpha_2 \end{vmatrix} \\
&= \pi(\sin\alpha_2\cos^2\alpha_1 - \sin\alpha_1\cos^2\alpha_2 + 2\sin\alpha_1 - 2\sin\alpha_2) \\
&= \pi(\cos\theta_1 + \cos\theta_2)(\cos\theta_1\cos\theta_2 + 1)
\end{aligned} \tag{16}$$

where we have used 15, 11 and 12 and 13. For the denominator, we get

$$\begin{aligned}
&\left.\frac{\partial(h,v,r_1,r_2)}{\partial(B,R,\alpha_1,\alpha_2)}\right|_{B=1,R=1} \\
&= \begin{vmatrix} -\frac{1}{2}\int_{\alpha_1}^{\alpha_2}\frac{\sin^2 t}{\cos t}\,dt & \sin\alpha_2 - \sin\alpha_1 & -\cos\alpha_1 & \cos\alpha_2 \\ \frac{\pi}{2}\int_{\alpha_1}^{\alpha_2}(3\cos^3 t - \cos t)\,dt & 3\pi\int_{\alpha_1}^{\alpha_2}\cos^3 t\,dt & -\pi\cos^3\alpha_1 & \pi\cos^3\alpha_2 \\ -\frac{1}{2}\cos\alpha_1 & \cos\alpha_1 & -\sin\alpha_1 & 0 \\ -\frac{1}{2}\cos\alpha_2 & \cos\alpha_2 & 0 & -\sin\alpha_2 \end{vmatrix} \\
&= \frac{\pi}{2}\Bigg[(\sin\alpha_2\cos^2\alpha_1 - \sin\alpha_1\cos^2\alpha_2 + 2\sin\alpha_1 - 2\sin\alpha_2)\left(\ln\frac{1+\sin\alpha_1}{\cos\alpha_1} - \ln\frac{1+\sin\alpha_2}{\cos\alpha_2}\right) - (\sin\alpha_1 - \sin\alpha_2)^2\Bigg] \\
&= \frac{\pi}{2}(\cos\theta_1 + \cos\theta_2)\Bigg[(\cos\theta_1\cos\theta_2 + 1)\left(\ln\frac{1+\sin\theta_1}{\cos\theta_1} + \ln\frac{1+\sin\theta_2}{\cos\theta_2}\right) - \cos\theta_1 - \cos\theta_2\Bigg]
\end{aligned} \tag{17}$$

where we have used $\int\sin^2 t/\cos t\,dt = \ln(\sec t + \tan t) - \sin t + C$. Inserting 16 and 17 into 14, cancelling the common factors and using the relation $-\ln((1+\sin x)/\cos x) = \ln\tan(x/2)$ finally gives that in the case III, the spring constant k is given by

$$\frac{2\pi\gamma}{k_1} = \ln\tan\frac{\theta_1}{2} + \ln\tan\frac{\theta_2}{2} + \frac{\cos\theta_1 + \cos\theta_2}{\cos\theta_1\cos\theta_2 + 1} \tag{18}$$

For the case II, we assume that the contact angle is fixed on the bottom substrate and that the contact radius is pinned on the top side. The process is otherwise identical and gives

$$\frac{2\pi\gamma}{k_1} = \ln\tan\frac{\theta_1}{2} + \ln\tan\frac{\theta_2}{2} + \frac{\cos\theta_1 + \cos\theta_2}{\cos\theta_1\cos\theta_2 + 1 + (\cot\theta_1 + \csc\theta_1\cos\theta_2)^2} \tag{19}$$

and for completeness, we will also give the expression for the case I as

$$\frac{2\pi\gamma}{k_1} = \ln\tan\frac{\theta_1}{2} + \ln\tan\frac{\theta_2}{2} + \frac{\cos\theta_1 + \cos\theta_2}{\cos\theta_1\cos\theta_2 + (\cos\theta_1 - \cos\theta_2)^2 - 3} \tag{20}$$

Summary of the Linear Spring Constants. We can now summarize all the linear spring constants in a simple expression that covers all the three cases

$$\frac{2\pi\gamma}{k_1} = \ln\tan\frac{\theta_1}{2} + \ln\tan\frac{\theta_2}{2} + \frac{\cos\theta_1 + \cos\theta_2}{\cos\theta_1\cos\theta_2 + 1 + f} \tag{21}$$

where f depends on the case

$$\begin{aligned}
&\text{Case I: } f = (\cos\theta_1 - \cos\theta_2)^2 - 4 \\
&\text{Case II: } f = (\cot\theta_1 + \csc\theta_1\cos\theta_2)^2 \\
&\text{Case III: } f = 0
\end{aligned} \tag{22}$$

Supporting Information shows that these expressions are equivalent to the expressions given by Kusumaatmaja & Lipowsky.[29]

DOI: 10.1021/acs.langmuir.9b00152
Langmuir 2019, 35, 7129−7135

Quadratic Spring Constants. As seen in Figure 1, the first-order approximation 1 underestimates the numerically computed force for both positive and negative Δh. This can be somewhat remedied by using the second-order approximation 2. Again, we use the implicit function theorem to find $\partial^2 F/\partial h^2$ and evaluate it at $B = 1$. In the case III, this gives the quadratic spring constant k_2 as

$$k_2 = -\frac{1}{2}\left(\frac{\partial^2 F}{\partial h^2}\right)_{V,r_1,r_2} = \pi\gamma\frac{X^3 + 3Y^2X - 3CY^3}{R(CY - X)^3} \quad (23)$$

where $X = \cos\theta_1 + \cos\theta_2$, $Y = \cos\theta_1 \cos\theta_2 + 1$ and $C = \ln\tan\theta_1/2 + \ln\tan\theta_2/2$. In the cases I and II, the rather lengthy expressions for k_2 are given in the Supporting Information

Snap-in Forces. Right before the snap-in, the drop is a spherical cap and has a height of h_S, which is given by

$$h_S = r_2\left(a - \frac{1}{a}\right), \text{ where } a = [D + \sqrt{1 + D^2}]^{1/3} \text{ and } D = \frac{3V}{\pi {r_2}^3} \quad (24)$$

assuming the drop was bound to the top substrate before the snap-in. $\Delta h = h_S - h_E$ and $k_{1,2}$ can now be put into either 1 or 2 to approximate the snap-in force.

RESULTS AND DISCUSSION

Recall that our initial aim was to find an analytical method for computing the snap-in forces of capillary bridges, with the purpose of linking the snap-in forces to the geometry of the capillary bridge—contact angle or contact radius at the substrate. We now have that analytical method and will compare these analytical approximations to numerical models and experimental data.

Comparison to Numerical Modeling. To compare the validity of the analytical approximation, the snap-in forces were also computed numerically using MATLAB software. Briefly, the numerical model finds the Kenmotsu parameters of the liquid bridge by numerically solving the system of eq 8. The equilibrium shape, which is incorrect only in its height, is used as the initial guess for the solver. All code to recreate all the figures can be downloaded from Zenodo.[36]

Figure 3 shows how the analytical approximation becomes increasingly accurate as either the contact angle is increased in the case II or the contact radius is decreased in the case III. Clearly, the analytical approximations become indistinguishable from a more accurate numerical solution when the contact radius is decreased or the contact angle is increased. The quadratic approximation is more accurate than the linear approximation for moderate contact angles and contact radii, but eventually diverges faster for small contact angles and large contact radii, because of the presence of the quadratic term.

To make the comparison of the models more concrete, we must define what we mean by a model being accurate. For example, we can say that an analytical model is accurate when the relative error between the analytical and the numerical model is less than 10%, that is, $|\log(F_{analytical}/F_{numeric})| < \log 1.1$. Figure 3 shows that the relative accuracy depends not only on the contact angle or the contact radius but also on the volume. When $V/{r_2}^3 = 100$, the linear model is accurate for contact angles above 159°, but the quadratic model is accurate for contact angles above 108°. On the other hand, when $V/{r_2}^3 = 5$, the linear model is accurate for contact angles above 172° and the quadratic model is accurate for contact angles above 143°.

Comparison to Experimental Data. For experimental validation of the model, we use published data from Liimatainen et al.[20] Figure 4 compares the experimental, numerical, and linear analytic and quadratic analytic force–distance relationship of a capillary bridge between two surfaces with pads. It shows that for small displacements, both analytical models approximate the numerical model, and the both agree reasonably well with the experimental curve, yet not perfectly.

Finally, Figure 5 compares the analytical, numerical, and experimental snap-in forces for mushroom-shaped pillars with varying radii. In the range of pillars tested, the linear analytical model is almost as good as the numerical model, except perhaps in the case of the largest of the pillars ($r_1/r_2 = 0.8$). The quadratic model is indistinguishable from the numerical

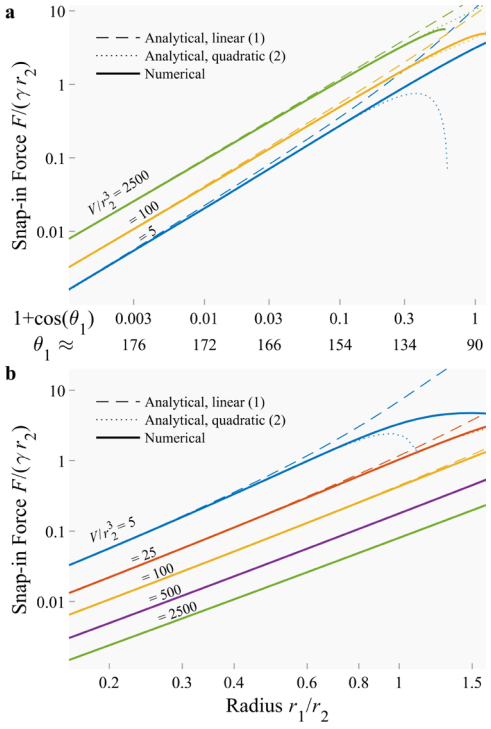

Figure 3. Comparison between numerically calculated and analytically approximated snap-in forces for (a) homogeneous substrates (case II); and (b) pads (case III). The analytical models become increasingly accurate when the contact angle increases or the contact radius decreases. Note that the scales on all axes are logarithmic and in (a), the work of adhesion $(1 + \cos\theta_1)$ values on the x-axis are accurate and the corresponding contact angle values approximate.

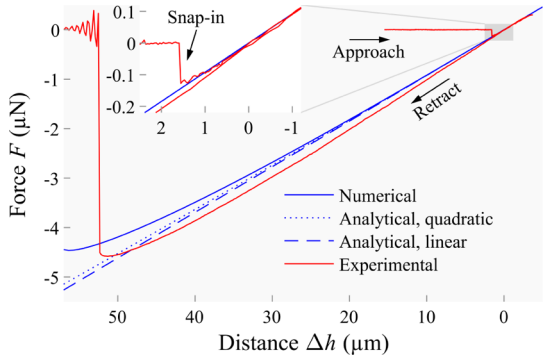

Figure 4. Analytical, numerical, and experimental force–distance curves in a case III type experiment. The experimental data is from Liimatainen et al.[20] In the experimental data, the distance at which $F = 0$ was taken as the equilibrium distance. The parameters were $r_1 = 10$ μm, $r_2 = 0.5$ mm, $V = 1.53$ μL, and $\gamma = 72$ mN/m.

DOI: 10.1021/acs.langmuir.9b00152
Langmuir 2019, 35, 7129–7135

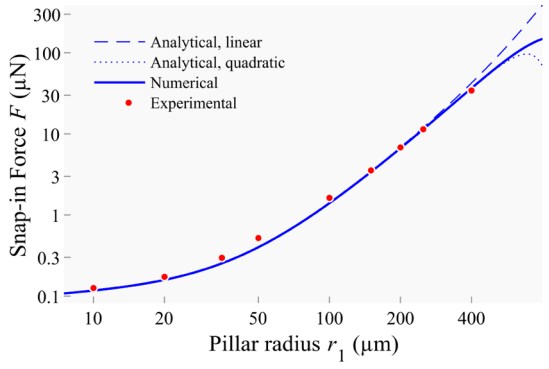

Figure 5. Comparison between analytical and numerical models and experiments in case III type experiments. The experimental data is from Liimatainen et al.[20] The parameters were r_2 = 0.5 mm, V = 1.53 μL, γ = 72 mN/m, and h_C = 1.2 μm. Note that both scales are logarithmic.

model in the range of the pillar radii tested. A small bend can be seen on the left side of Figure 5 for all models. This bend is due to the cap thickness of the mushroom-shaped pillars in the experiments. After snap-in, the contact line first spreads on the top of the cap, and then spreads along the sides of the cap, pinning to the bottom edge of the cap. The contact line pinning to the bottom of the cap can be accounted for by adding the thickness of the cap h_C to the snap-in distance, that is, $\Delta h = h_S - h_E + h_C$. Without this correction, there is no bend in the models and none of the model approximates the experimental data well. Nevertheless, the analytical and numerical models agree perfectly with each other in the small contact radius limit.

Summary and Conclusions. In summary, we now have an analytical method for calculating approximately the snap-in forces of liquid drops that captures a body of experimental data. It is therefore a valuable addition to the toolbox of a scientist working on normal forces of liquid drops.

It is worth pointing out that the theory was only compared to the experiments for the case III because of the unavailability of high-quality experimental data from the cases I and II. One of the difficulties of such measurements is that it is difficult to measure optically contact angles beyond 150°. Unfortunately, this super liquid-repellent limit is where one would expect the analytical models to be more accurate, according to Figure 3. A second potential difficulty is that most studies have focused on water as the liquid and all substrates with water contact angle beyond 130° have some kind of micro-/nanotopography. On such a roughness, the radial or axial contact line position may be uneven, that is, the axial symmetry assumption may be violated.

Finally, we have so far not considered receding contact angles at all, even though it has been argued[18] that the receding contact angle is a more relevant characteristic of a super liquid-repellent surface because it puts an upper bound on the sliding angle. Receding contact angle can, in principle, be obtained from force measurements, if the probe is retracted far enough that the contact line de-pins and starts retracting. Measuring the minimum force during retraction or the force right before pull-off (capillary bridge failure) has been proposed as an alternative to measuring receding contact angles.[20] There are difficulties in applying the approach developed in this paper to compute the pull-off forces: (1) the linearized curve cannot be used to find the distance at which the force is at minimum. (2) The Δh is larger during pull-off than during snap-in, so the analytical models introduce more errors.

The previous difficulties immediately suggest the following approach: instead of snap-in or pull-off forces, one could measure the slope of the force−distance curve at the equilibrium distances during approach and retraction, respectively. Equation 21 could then be used to relate the slopes to the contact angles at the substrates. Figure 6 shows a simulated experiment and how the contact angles could be extracted from such data. In such an experiment, one should squeeze the bridge enough during the approach. This would guarantee that during retraction, when the equilibrium distance is reached, the contact line has already depinned and is receding.

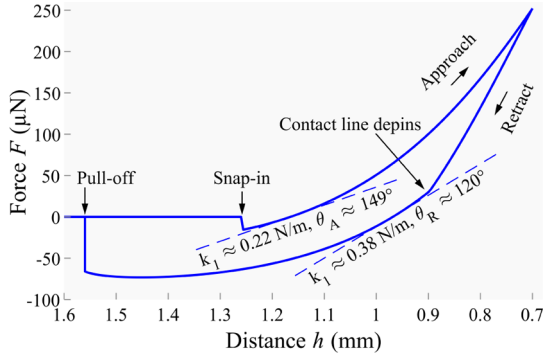

Figure 6. Simulated experiment demonstrating how both advancing and receding contact angles can be extracted from the spring constants. The force−distance curve was computed numerically, using parameters r_2 = 0.5 mm, V = 1.53 μL, γ = 72 mN/m, advancing contact angle θ_A = 150°, and receding contact angle θ_R = 120°. To extract the contact angles from the data: (1) find the slopes of the tangent lines at the equilibrium distances (F = 0) during approach and retraction; (2) find a spherical segment that has the prescribed V, r_2, and k_1; k_1 given by 19. The spherical segment gives θ_1.

■ ASSOCIATED CONTENT

Supporting Information

The Supporting Information is available free of charge on the ACS Publications website at DOI: 10.1021/acs.langmuir.9b00152.

Maple software worksheet showing the derivation of all the equations (PDF)

■ AUTHOR INFORMATION

Corresponding Author

*E-mail: veikko.sariola@tuni.fi.

ORCID

Veikko Sariola: 0000-0001-8307-6120

Author Contributions

V.S. is the sole author of the manuscript.

Funding

This work was supported by the Academy of Finland (grant: #299087).

Notes

The author declares no competing financial interest.

DOI: 10.1021/acs.langmuir.9b00152
Langmuir 2019, 35, 7129−7135

■ ACKNOWLEDGMENTS

Dr. Ville Liimatainen kindly communicated the experimental data in Figures 4 and 5. Dr. Ville Liimatainen, Dr. Vipul Sharma, Dr. Maja Vuckovac, Dr. Matti Hokkanen and Anastasia Koivikko kindly read and commented on the draft of this manuscript. Any errors or mistakes remain my sole responsibility.

■ REFERENCES

(1) Lin, W.; Patra, S. K.; Lee, Y. C. Design of Solder Joints for Self-Aligned Optoelectronic Assemblies. *IEEE Trans. Compon., Packag., Manuf. Technol., Part B* **1995**, *18*, 543−551.
(2) Goldman, L. S. A Heuristic Force-Height Equation for Molten Axisymmetric Solder Joints. *Proceedings IEEE 43rd Electronic Components and Technology Conference*; IEEE, 1993; pp 1120−1124
(3) Yasuda, K.; Kim, J.-M.; Yasuda, M.; Fujimoto, K. Formation of a Self-Interconnected Joint Using a Low-Melting-Point Alloy Adhesive. *Mater. Trans.* **2004**, *45*, 799−805.
(4) Sato, K.; Ito, K.; Hata, S.; Shimokohbe, A. Self-alignment of microparts using liquid surface tension—behavior of micropart and alignment characteristics. *Precis. Eng.* **2003**, *27*, 42−50.
(5) Sariola, V.; Jääskeläinen, M.; Zhou, Q. Hybrid Microassembly Combining Robotics and Water Droplet Self-Alignment. *IEEE Trans. Robot.* **2010**, *26*, 965−977.
(6) Mastrangeli, M.; Zhou, Q.; Sariola, V.; Lambert, P. Surface Tension-Driven Self-Alignment. *Soft Matter* **2017**, *13*, 304−327.
(7) Aoyama, H.; Hiraiwa, S.; Iwata, F.; Fukaya, J.; Sasaki, A. Miniature Robot with Micro Capillary Capturing Probe. *Proceedings 6th International Symposium Micro Machine & Human Science*; IEEE, 1995; pp 173−178.
(8) Lambert, P.; Delchambre, A. A Study of Capillary Forces as a Gripping Principle. *Assem. Autom.* **2005**, *25*, 275−283.
(9) Sariola, V.; Liimatainen, V.; Tolonen, T.; Udd, R.; Zhou, Q. Silicon Capillary Gripper With Self-Alignment Capability. *IEEE International Conference on Robotics and Automation*, 2011; pp 4098−4103.
(10) Vogel, M. J.; Steen, P. H. Capillarity-Based Switchable Adhesion. *Proc. Natl. Acad. Sci. U.S.A.* **2010**, *107*, 3377−3381.
(11) Bocquet, L.; Charlaix, E.; Ciliberto, S.; Crassous, J. Moisture-Induced Ageing in Granular Media and the Kinetics of Capillary Condensation. *Nature* **1998**, *396*, 735−737.
(12) Pakarinen, O. H.; Foster, A. S.; Paajanen, M.; Kalinainen, T.; Katainen, J.; Makkonen, I.; Lahtinen, J.; Nieminen, R. M. Towards an Accurate Description of the Capillary Force in Nanoparticle-Surface Interactions. *Modell. Simul. Mater. Sci. Eng.* **2005**, *13*, 1175−1186.
(13) Wexler, J. S.; Heard, T. M.; Stone, H. A. Capillary Bridges between Soft Substrates. *Phys. Rev. Lett.* **2014**, *112*, 066102.
(14) Feiler, A. A.; Stiernstedt, J.; Theander, K.; Jenkins, P.; Rutland, M. W. Effect of Capillary Condensation on Friction Force and Adhesion. *Langmuir* **2007**, *23*, 517−522.
(15) Mastrangeli, M. The Fluid Joint: The Soft Spot of Micro- and Nanosystems. *Adv. Mater.* **2015**, *27*, 4254−4272.
(16) Attard, P.; Miklavcic, S. J. Effective Spring Constant of Bubbles and Droplets. *Langmuir* **2001**, *17*, 8217−8223.
(17) Men, Y.; Zhang, X.; Wang, W. Capillary Liquid Bridges in Atomic Force Microscopy: Formation, Rupture, and Hysteresis. *J. Chem. Phys.* **2009**, *131*, 184702.
(18) Butt, H.-J.; Roisman, I. V.; Brinkmann, M.; Papadopoulos, P.; Vollmer, D.; Semprebon, C. Characterization of Super Liquid-Repellent Surfaces. *Curr. Opin. Colloid Interface Sci.* **2014**, *19*, 343−354.
(19) Escobar, J. V.; Castillo, R. Force of Adhesion on Super-solvophobic Surfaces: The Role of Capillary Necks. *Phys. Rev. E* **2016**, *93*, 022804.
(20) Liimatainen, V.; Vuckovac, M.; Jokinen, V.; Sariola, V.; Hokkanen, M. J. M. J.; Zhou, Q.; Ras, R. H. A. Mapping Microscale Wetting Variations on Biological and Synthetic Water-Repellent Surfaces. *Nat. Commun.* **2017**, *8*, 1798.
(21) Zhang, Y.; Park, S.; Liu, K.; Tsuan, J.; Yang, S.; Wang, T.-H. A Surface Topography Assisted Droplet Manipulation Platform for Biomarker Detection and Pathogen Identification. *Lab Chip* **2011**, *11*, 398−406.
(22) Samuel, B.; Zhao, H.; Law, K.-Y. Study of Wetting and Adhesion Interactions between Water and Various Polymer and Superhydrophobic Surfaces. *J. Phys. Chem. C* **2011**, *115*, 14852−14861.
(23) Liu, K.; Vuckovac, M.; Latikka, M.; Huhtamäki, T.; Ras, R. H. A. TrickyImproving surface-wetting characterization. *Science* **2019**, *363*, 1147−1148.
(24) Saksono, P. H.; Perić, D. On finite element modelling of surface tension Variational formulation and applications - Part I: Quasistatic problems. *Comput. Mech.* **2005**, *38*, 265−281.
(25) Brakke, K. A. The Surface Evolver. *Exp. Math.* **1992**, *1*, 141−165.
(26) Pan, H.; Choi, Y.-K.; Liu, Y.; Hu, W.; Du, Q.; Polthier, K.; Zhang, C.; Wang, W. Robust Modeling of Constant Mean Curvature Surfaces. *ACM Trans. Graph.* **2012**, *31*, 1−11.
(27) Delaunay, C. H. Sur La Surface de Révolution Dont La Courbure Moyenne Est Constante. *J. Math. Pures Appl.* **1841**, *6*, 309−314.
(28) Kenmotsu, K. Surfaces of Revolution with Prescribed Mean Curvature. *Tohoku Math. J.* **1980**, *32*, 147−153.
(29) Kusumaatmaja, H.; Lipowsky, R. Equilibrium Morphologies and Effective Spring Constants of Capillary Bridges. *Langmuir* **2010**, *26*, 18734−18741.
(30) Meurisse, M. H.; Querry, M. Squeeze Effects in a Flat Liquid Bridge Between Parallel Solid. *J. Tribol.* **2006**, *128*, 575−584.
(31) Petkov, P. V.; Radoev, B. P. Statics and Dynamics of Capillary Bridges. *Colloid. Surf. Physicochem. Eng. Asp.Colloid. Surf. Physicochem. Eng. Asp.* **2014**, *460*, 18−27.
(32) Vogel, T. I. Stability of a Liquid Drop Trapped between Two Parallel Planes. *SIAM J. Appl. Math.* **1987**, *47*, 516−525.
(33) Heinrich, S. M.; Shakya, S.; Wang, Y.; Lee, P. S.; Schroeder, S. A. Improved Yield and Performance of Ball-Grid Array Packages: Design and Processing Guidelines for Uniform and Nonuniform Arrays. *IEEE Trans. Components, Packag. Manuf. Technol. Part B* **1996**, *19*, 310−319.
(34) Yost, B.; McGroarty, J.; Borgesen, P.; Li, C.-Y. Shape of a Nonaxisymmetric Liquid Solder Drop Constrained by Parallel Plates. *IEEE Trans. Compon., Hybrids, Manuf. Technol.* **1993**, *16*, 523−526.
(35) Buckingham, E. On Physically Similar Systems; Illustrations of the Use of Dimensional Equations. *Phys. Rev.* **1914**, *4*, 345−376.
(36) Sariola, V. Code Related to the Paper: "Analytical Expressions for Spring Constants of Capillary Bridges and Snap-in Forces of Hydrophobic Surfaces". *Zenodo* **2019**, DOI: 10.5281/zenodo.2633991.

DOI: 10.1021/acs.langmuir.9b00152
Langmuir 2019, 35, 7129−7135